Journal for ImmunoTherapy of Cancer

Integrated immunological analysis of a successful conversion of locally advanced hepatocellular carcinoma to resectability with neoadjuvant therapy

Won Jin Ho ,[1] Gaurav Sharma,[2] Qingfeng Zhu,[3] Genevieve Stein-O'Brien,[4] Jennifer Durham,[1] Robert Anders,[3] Aleksandra Popovic,[1] Guanglan Mo,[1] Ihab Kamel,[5] Matthew Weiss,[6] Elizabeth Jaffee,[1] Elana J Fertig,[2,4] Mark Yarchoan[1]

To cite: Ho WJ, Sharma G, Zhu Q, *et al*. Integrated immunological analysis of a successful conversion of locally advanced hepatocellular carcinoma to resectability with neoadjuvant therapy. *Journal for ImmunoTherapy of Cancer* 2020;**8**:e000932. doi:10.1136/jitc-2020-000932

► Additional material is published online only. To view please visit the journal online (http://dx.doi.org/10.1136/jitc-2020-000932).

Accepted 26 August 2020

For numbered affiliations see end of article.

Correspondence to
Mark Yarchoan;
mark.yarchoan@jhmi.edu

ABSTRACT

Hepatocellular carcinoma (HCC) is the fourth leading cause of cancer death worldwide with a minority of patients being diagnosed early enough for curative-intent interventions. We report the first use of preoperative cabozantinib plus nivolumab to successfully downstage what presented as unresectable HCC as part of an ongoing phase 1b study. Preoperative treatment with cabozantinib and nivolumab led to >99% reduction in alpha-fetoprotein, −37.3% radiographic reduction by RECIST 1.1 and a near complete pathologic response (80% to 100% necrosis). An integrated immunological analysis was performed on the post-treatment surgical tumor sample and matched pre-treatment and post-treatment peripheral blood samples with high-dimensional imaging and cytometry techniques. Bayesian non-negative matrix factorization (CoGAPS, Coordinated Gene Activity in Pattern Sets) and self-organizing map (FlowSOM) algorithms were used to distinguish changes in functional markers across cellular neighborhoods in the single cell data sets. Brisk immunological infiltration into the tumor microenvironment was observed in non-random, organized cellular neighborhoods. Systemically, combination therapy led to marked promotion of effector cytotoxic T cells and effector memory helper T cells. Natural killer cells also increased with therapy. The patient remains without disease recurrence and with a normal alpha-fetoprotein approximately 2 years from presentation. Our study provides proof-of-concept that borderline resectable or locally advanced HCC warrants consideration of downstaging with effective neoadjuvant systemic therapy for subsequent curative resection.

INTRODUCTION

Hepatocellular carcinoma (HCC) is the fourth leading cause of cancer death worldwide. The estimated 5-year survival rate for HCC is 18%, reflecting that a minority of patients are diagnosed early enough to be candidates for curative-intent therapies such as surgical resection, ablation, or liver transplantation.[1] Patients who are not transplant candidates and who have tumors outside of resection criteria at presentation are generally treated with locoregional therapy or systemic therapy with palliative intent. The utility of preoperative transcatheter arterial chemoembolization for HCC remains controversial at best with uncontrolled series as well as randomized controlled trial studies having demonstrated associations with an increased risk of postoperative disease recurrence.[2–6] Moreover, the use of systemic therapy to downstage HCC has not been feasible due to the low response rate of sorafenib, which was until recently the only approved systemic therapy. Novel combinations of targeted agents and inhibitors of the programmed cell death protein 1 (PD-1) axis demonstrate response rates of approximately 30% in HCC,[7–9] which is similar to tumor types for which neoadjuvant systemic therapy is standard practice in borderline resectable or locally advanced cases.[10 11] We report the first patient treated on a protocol of neoadjuvant cabozantinib plus nivolumab in borderline resectable or locally advanced HCC (NCT03299946) who was successfully converted to a resection candidate, with prolonged disease-free survival after resection. Cabozantinib is a tyrosine kinase inhibitor (TKI) with potent activity against VEGFR2, MET, AXL, and other kinases. Nivolumab is an inhibitor of the PD-1 immune checkpoint.

Recent progress in single-cell technologies, for example, in suspension cytometry, sequencing, imaging methods, and analytical algorithms, have enabled unprecendented depth and breadth to studying immunologic phenomena. For example, imaging mass cytometry and spatial analysis tools have recently emerged as powerful tools for evaluating spatial coordination of cells within the tumor microenvironment.[12] We have recently developed and demonstrated the

utility of a non-negative matrix factorization algorithm, Coordinated Gene Activity in Pattern Sets (CoGAPS), to discover meaningful cell types and states from single-cell data sets.[13] Whereas a clustering algorithm based on Self-Organizing Map, for example, FlowSOM,[14] limits cells to a single cluster, protein markers from CoGAPS can associate cells with both functional markers and discrete cell types. To profile the immunological state underlying the clinical outcome in response to the novel combination of cabozantinib and nivolumab, we employ these highly multiplexed imaging and cytometry assays along with the computational tools to provide an in-depth, unbiased analysis of the immunological response.

RESULTS

Clinical response

A man in his early 70s with a history of hepatitis C cirrhosis (Child Pugh A) presented with a 5.8 cm hypervascular and infiltrative lesion in his inferior right hepatic lobe with extension into the porta hepatis, and tumor thrombus extending into the right anterior portal vein, consistent with HCC. Also in the right lobe was a second focus of enhancement that was poorly defined but most consistent with a satellite lesion. The disease was deemed unresectable based on Barcelona Clinic Liver Cancer criteria.[15] His alpha-fetoprotein (AFP) increased from 17,528 ng/mL at the time of presentation to 30,070 ng/mL at the time of multidisciplinary evaluation 12 days later (AFP doubling time of approximately 15 days). He was treated with cabozantinib 40 mg oral daily for 2 weeks (cabozantinib lead in), followed by 8 weeks of concurrent cabozantinib 40 mg plus nivolumab (240 mg every 2 weeks for a total of four doses). Additional details related to the clinical trial are available in the online supplemental information. The subject's AFP declined with therapy to 12.9 ng/mL (>99% reduction from treatment baseline) and the patient experienced a 37.3% radiographic reduction in his lesions by RECIST 1.1 (figure 1A,B).

Approximately 4 weeks after his last dose of nivolumab, he underwent a right hepatectomy and cholecystectomy. The operation itself was uneventful, although the high bifurcation of the portal vein and the patient's original tumor thrombus and macrovascular invasion made it difficult to get around the right portal vein during the surgical operation. His postoperative course was complicated by significant output from his Jackson-Pratt drain, and the patient received intermittent doses of intravenous furosemide to manage the drain output. In the opinion of the treating surgical oncologist (MJW), there were no discernable adverse events from neoadjuvant therapy on the perioperative course, and the patient's wound healing was normal. Pathology from the surgical resection

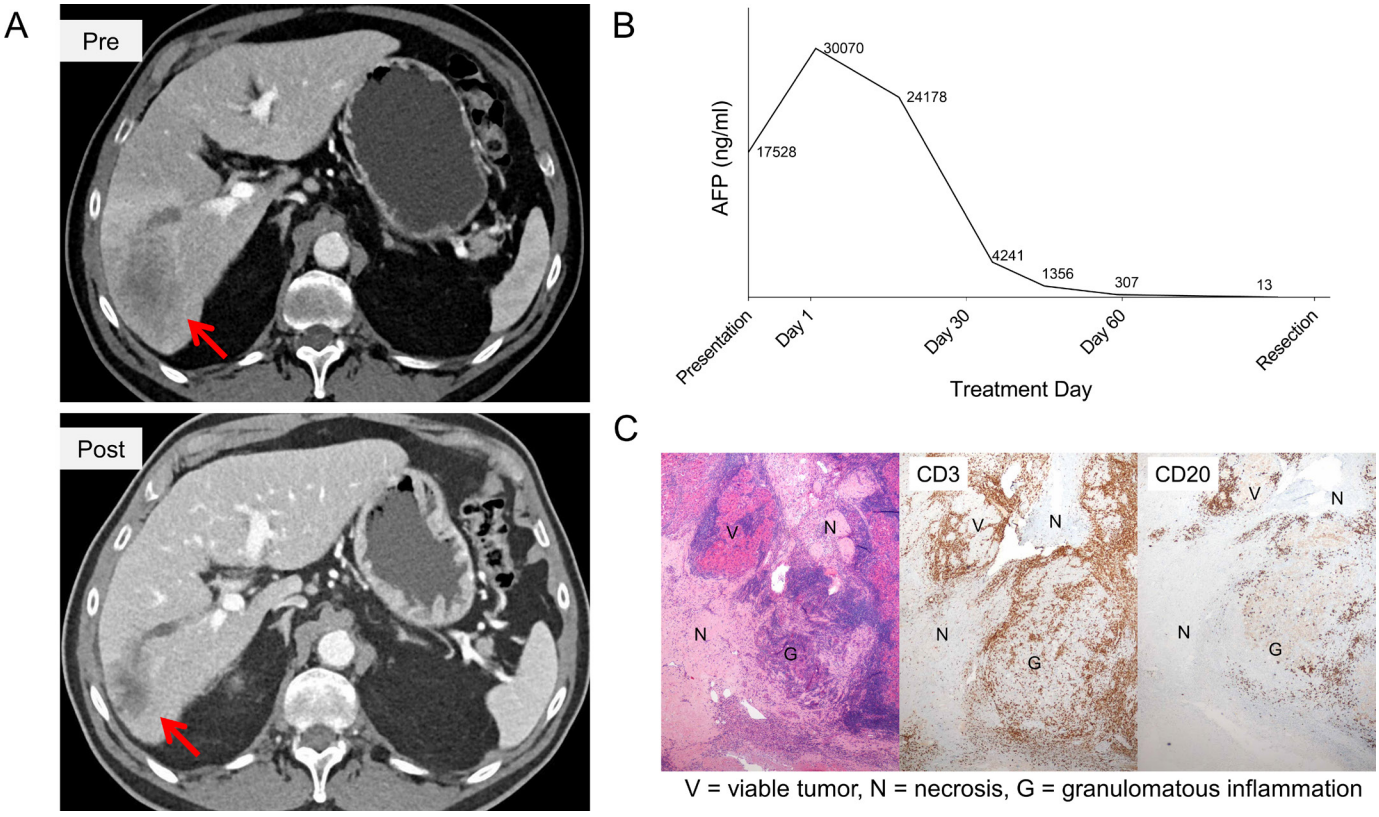

Figure 1 Clinical response to neoadjuvant cabozantinib and nivolumab. Neoadjuvant therapy resulted in (A) tumor downstaging, with the dominant infiltrative lesion decreasing from 5.81 cm to 3.64 cm in maximum diameter (B) marked reduction in AFP, and (C) tumor necrosis and brisk immune infiltration by immunohistochemistry with CD3+T cells and CD20+B cells. AFP, alpha-fetoprotein.

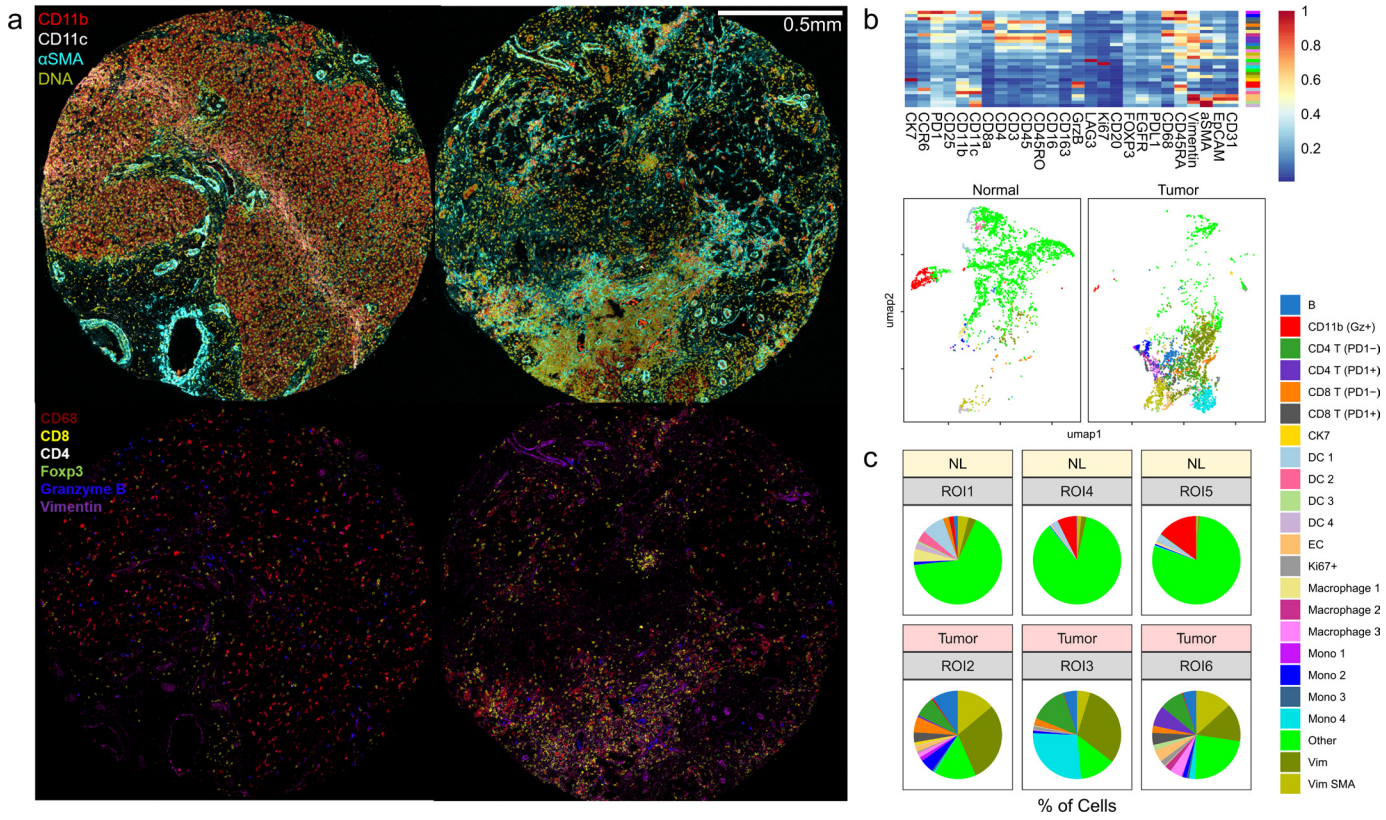

Figure 2 Neoadjuvant cabozantinib plus nivolumab results in dramatic immunological response in the tumor microenvironment. (A) Representative pictures of imaging mass cytometry of normal liver cores (left) and cores from surgically resected tumor samples post systemic therapy (right). Normal hepatocytes demonstrate mild CD11b positivity. Connective tissue deposition (aSMA) is higher within the tumor sample. Post-treatment core demonstrates a focus of dense immune infiltration (bottom right). (B) Results from FlowSOM clustering analysis is visualized as a heatmap and UMAP. (C) Tumor microenvironment profiles in three normal liver regions and three post-treatment tumor regions are compared. A total of 20,631 cells for normal and 39,066 cells for tumor regions are analyzed. aSMA, alpha-smooth muscle actin; DC, dendritic cells; EC, endothelial cells; Gz, granzyme B; Mono, monocytes; Vim, vimentin.

returned as clear margins with significant treatment effect. One of the lesions was 100% necrotic; the other lesion was more than 80% necrotic and residual areas of tumor were associated with a brisk immune infiltration (figure 1C). He did not receive any adjuvant therapy, but did receive surveillance imaging with CT scans every 3 months. He remains without disease recurrence (online supplemental figure 1) with excellent performance status (Eastern Cooperative Oncology Group (ECOG) Scale: 0), normal liver function, and a normal AFP over 2 years from presentation (online supplemental table 1).

IMMUNOLOGIC ANALYSIS

To understand the immunologic profiles underlying the clinical response, immune infiltration within the tumor microenvironment (TME) was first evaluated with multiplexed imaging mass cytometry (IMC) (figure 2A; zoomed-in image, online supplemental figure 3). To maximize the area of analysis, data was acquired from three large diameter (1.5 mm) cores from the surgical tumor sample. Since the pre-treatment biopsy was only a core biopsy sample, a normal liver sample was used as an independent reference. Clustering analysis with FlowSOM algorithm of the single cells segmented from the images revealed markedly high abundances of immune cells, including CD4+T, CD8+T, and myeloid populations (figure 2B,C). We further validated the treatment-mediated increase in the presence of immune cells in the TME by comparing immune cell densities with single immunohistochemistry against CD3, CD8, and CD20 (online supplemental figure 3). As expected, the treatment led to a substantial increase in CD8 and CD20 positive cells. To delineate whether these cell types exhibited particular spatial relationships, two analytical methods were used on detected immune cell type patterns from the IMC data set (figure 3): neighborhood analysis, that is, how each cell type spatially relates to other cell types, performed using histoCAT;[16] and autocorrelation statistics, that is, whether each cellular pattern is distributed in a coordinated manner, enabled by quantitative cell pattern detection with CoGAPS. Within the treated HCC, a significantly organized cellular neighborhood among CD8+T cell, CD4+T cell, B cell, and myeloid cell patterns were present. Also, spatial proximity between a stromal pattern (alpha-smooth muscle actin, aSMA) and the prominent immune cell neighborhood was notable.

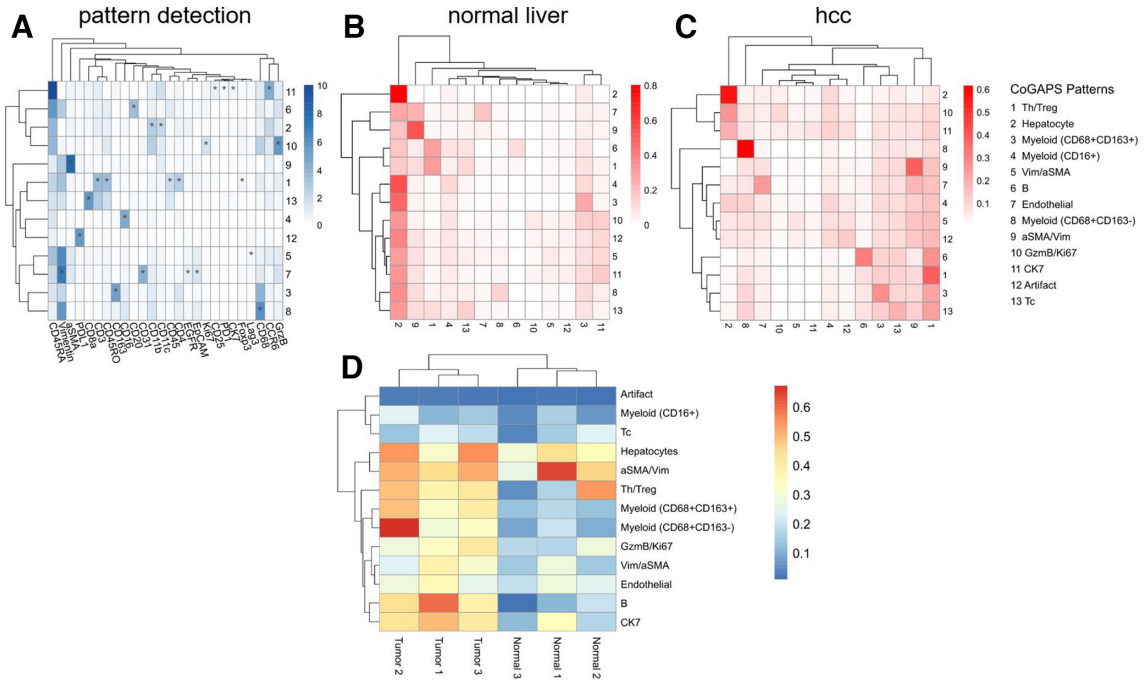

Figure 3 Neighborhood analysis of normal and post-treatment liver cores identifies distinct spatial neighborhoods in hepatocellular carcinoma treated with a combination of cabozantinib and nivolumab. (A) Pattern detection using Coordinated Gene Activity in Pattern Sets (CoGAPS) recapitulated major clusters identified by FlowSOM. Resulting pattern weights for each marker are shown as a heatmap. Markers that are driving the patterns according to the CoGAPS PatternMarker statistic are also marked with asterisks. (B and C) Heatmap of the cellular neighborhoods in normal liver (B) and HCC (C) regions. (D) Results of spatial autocorrelation for three normal liver and three HCC regions. GzmB, granzyme B; Tc, cytotoxic T cells; Th/Treg, helper T cells/regulatory T cells; Vim, vimentin.

Strong spatial autocorrelations were noted for immune cell patterns within the treated tumor microenvironment, especially for B cells, helper T cells, regulatory T cells, and CD68+CD163− myeloid cells. As expected, neighborhoods were only centered around hepatocytes and no significant autocorrelations could be identified in the normal liver. These results suggested that not only does cabozantinib-nivolumab combination lead to successful immune cell recruitment but also that the co-infiltration of lymphoid and myeloid cells occurs in a non-random, coordinated manner in relation to each other and to the stroma.

To evaluate the systemic immunologic effects related to combination of cabozantinib and nivolumab, we also assessed the peripheral immune profiles at baseline and post-treatment settings by suspension mass cytometry (CyTOF). Also, to compare the findings with the local immune response, we concurrently profiled the tumor-infiltrating immune cells using the same CyTOF panel (figure 4). In general, T cell abundances at earlier differentiation states, for example, naïve and central memory, decreased while effector memory and effector populations increased. Furthermore, marked systemic promotion of effector cytotoxic T cells mirrored the dominant cell type present locally. There was also an overall decrease in regulatory T cells. Most notably, the relative abundance of natural killer (NK) cells increased with therapy.

All methods for the immunological analysis are described in detail in the online supplemental information).

DISCUSSION

The use of systemic therapies in HCC are typically restricted to patients with advanced HCC, or intermediate stage HCC that is not amenable to locoregional therapies. This first case provides support for the idea that patients who have HCC that is beyond standard resection criteria can be downstaged with upfront use of novel and highly active systemic therapy, with long-term disease-free survival. Additional research is needed to identify predictive biomarkers to select patients for the approach described in this case. The described case is consistent with the observations of Kaseb and colleagues, who demonstrated a high rate of pathologic responses in patients receiving neoadjuvant nivolumab with or without ipilimumab.[17] However, in contrast to this prior report, our patient had unresectable disease at presentation, and demonstrates the potential for tumor downstaging in addition to pathologic responses. Furthermore, we are the first to test the combination of a TKI with immunotherapy in the preoperative setting in HCC. Based on this experience, the results of our phase 1b are highly anticipated. It is worth noting, however, that this is a single case experience, and in fact, there have been extraordinary responses to even sorafenib, with which curative resection was performed successfully for locally advanced disease at presentation.[18]

The use of systemic therapy in the neoadjuvant setting offers a tremendous research opportunity to better elucidate mechanisms of response and resistance in HCC. In

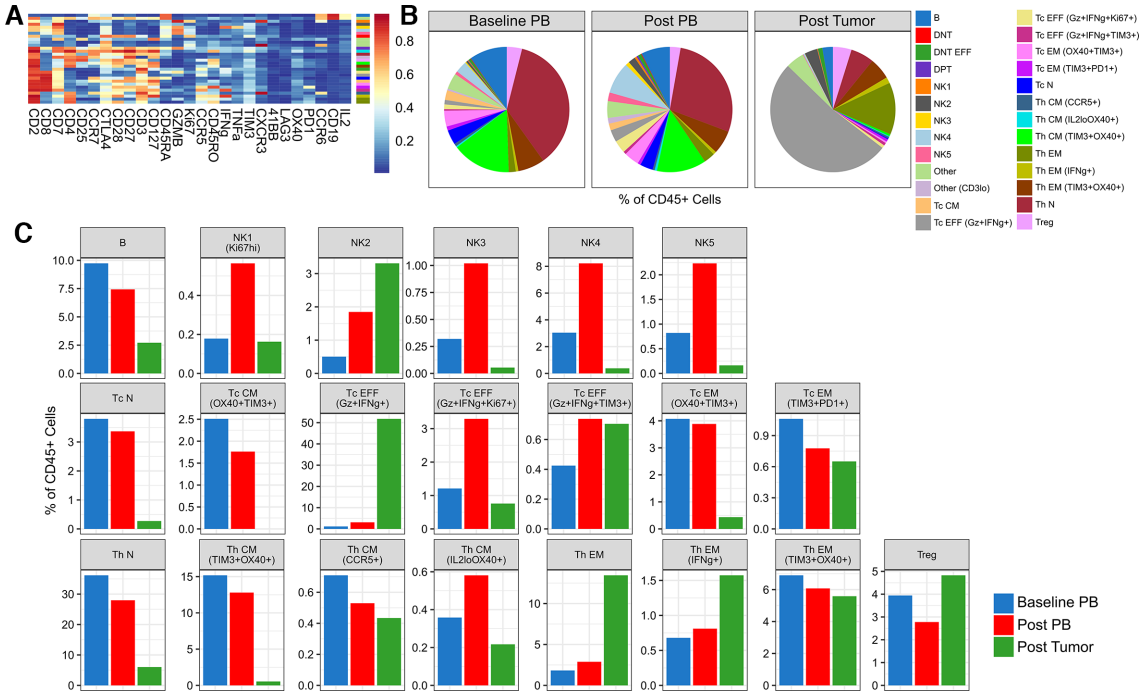

Figure 4 Differences in the immune profiles of baseline and post-treatment specimens are revealed by CyTOF. (A) Heatmap of the normalized expression for all markers used during FlowSOM clustering for all CD45+ cells acquired from baseline and post-treatment samples using a T cell-oriented CyTOF panel. The color bar to the right of the expression heatmap describes how each cell type has been annotated. (B) Pie and (C) bar plots showing the differences in abundance of the resulting immune cell clusters as a percentage of total CD45+ cells, comparing baseline peripheral blood (PB), post-treatment PB, and post-treatment surgical tumor sample from the patient. CM, central memory; DNT, double negative T cells; DPT, double positive T cells; EFF, effector; EM, effector memory; N, naïve; NK, natural killer; Tc, cytotoxic T cells; Th, helper T cells; Treg, regulatory T cells.

addition to characterizing an inflamed TME by robust presence of immune cells, the importance of spatial relationships among the infiltrating immune cells are increasingly being recognized. Recent studies including our own have reported the presence of distinctive immune cell aggregates, for example, tertiary lymphoid structures, within the TME in the context of immunotherapy.[19 20] Our analysis demonstrating high neighborhood and autocorrelation statistics among the lymphoid cells lend further support for the importance of such structures in immunologically active TME for therapeutic efficacy. Moreover, our multiplexed imaging with IMC added an additional depth to these observations that important spatial relationships also involve myeloid cells and stromal components. We also identified key systemic immunologic changes induced by the combination of cabozantinib and nivolumab. T cell related changes are consistent with the well-established effects of anti-PD1 therapies in promoting T cell activation.[21 22] It is, however, unclear as to why CD8+ cell density but not CD3+ cell density increases when comparing post-treatment versus pre-treatment settings. Since CD3-positivity includes a variety of T cell subtypes including regulatory T cells, one can speculate that the treatment is able to influence which functional subtype of T cells would dominate within the TME. Regarding NK cells, interestingly, there were notable increases in their abundance, supporting the hypothesis that this combination may elicit antitumor effects in part through the action of NK cells.[23] Overall, further validation of these trends observed is anticipated pending the analysis of the entire trial. Methodologically, our study also demonstrates for the first time that CoGAPS algorithm enables the following two applications: (1) CoGAPS can recover cell type patterns from mass cytometry data sets that are consistent with FlowSOM and (2) CoGAPS pattern intensities for each cell provides continuous data that can be leveraged for autocorrelation statistics. The results from this first patient will be significantly enhanced by the final results of the trial and thus analysis of responders versus non-responders.

In conclusion, the striking clinical response to the novel combination of cabozantinib and nivolumab observed in this patient's scenario suggests that unresectable HCC may warrant consideration for attempted downstaging with effective preoperative systemic therapy. Our demonstrated approach to perform an unbiased integrated analysis of both local and systemic immune responses with complementary methodologies will be applied to every patient in the ongoing trial to accelerate discovery.

Author affiliations
[1]Department of Oncology, Johns Hopkins Medicine Sidney Kimmel Comprehensive Cancer Center, Baltimore, Maryland, USA
[2]Division of Biostatistics and Bioinformatics, Johns Hopkins Medicine Sidney Kimmel Comprehensive Cancer Center, Baltimore, Maryland, USA
[3]Department of Pathology, Johns Hopkins University School of Medicine, Baltimore, Maryland, USA

[4]McKusick-Nathans Institute of Genetic Medicine, Johns Hopkins University School of Medicine, Baltimore, Maryland, USA
[5]Department of Radiology and Radiological Science, Johns Hopkins University School of Medicine, Baltimore, Maryland, USA
[6]Department of Surgery, Johns Hopkins University School of Medicine, Baltimore, Maryland, USA

Twitter Won Jin Ho @wonjinho1

Acknowledgements Mass cytometry data were acquired at the University of Maryland School of Medicine Center for Innovative Biomedical Resources (CIBR) Flow Cytometry and Mass Cytometry Core Facility, Baltimore, Maryland.

Contributors Conception and design: M Yarchoan. Development and methodology: W Ho, G Sharma, G Stein-O'Brien, EJ Fertig, G Mo, J Durham, EM Jaffee, and M Yarchoan. Acquisition of data: W Ho, G Mo, A Popovic, M Weiss, Q Zhu, R Anders, and M Yarchoan. Analysis and interpretation of data: W Ho, A Popovic, I Kamel, G Sharma, EJ Fertig, Q Zhu, R Anders, EM Jaffee, and M Yarchoan. Writing, review, and/or revision of the manuscript: All authors. Administrative, technical, or material support: J Durham, EM Jaffee, and M Yarchoan.

Funding Funding for this clinical trial were provided by Exelixis and Bristol Myers Squibb (to MY). Additional research support was provided by the National Cancer Institute Specialized Program of Research Excellence (SPORE) in Gastrointestinal Cancers (P50 CA062924), the NIH Center Core Grant (P30 CA006973), and the Emerson Collective Cancer Research Fund (640183).

Competing interests WH is a co-inventor of patents with potential for receiving royalties from Rodeo Therapeutics unrelated to the current study. MY reports receiving a commercial research grant from Bristol Myers Squibb, Exelixis, and Merck & Co and is a consultant/advisory board member for Eisai and Exelixis. EJF is a consultant for Champions Oncology. EMJ reports receiving a commercial research grant from Bristol Myers Squibb, Aduro Biotech, and Amgen, has ownership interest (including stock, patents, and so on) in Aduro Biotech, and is a consultant/advisory board member for CStone, Dragonfly, Genocea, and Adaptive Biotechnologies.

Patient consent for publication Not required.

Ethics approval The evaluation of clinical samples was performed in accordance with the protocols approved by the Johns Hopkins Institutional Review Board (IRB). All specimens were obtained with written patient consent (IRB00149350).

Provenance and peer review Not commissioned; externally peer reviewed.

ORCID iD
Won Jin Ho http://orcid.org/0000-0003-2644-5086

REFERENCES

1 Villanueva A. Hepatocellular carcinoma. *N Engl J Med* 2019;380:1450–62.
2 Sasaki A, Iwashita Y, Shibata K, *et al*. Preoperative transcatheter arterial chemoembolization reduces long-term survival rate after hepatic resection for resectable hepatocellular carcinoma. *Eur J Surg Oncol* 2006;32:773–9.
3 Wu CC, Ho YZ, Ho WL, *et al*. Preoperative transcatheter arterial chemoembolization for resectable large hepatocellular carcinoma: a reappraisal. *Br J Surg* 1995;82:122–6.
4 Amisaki M, Honjo S, Morimoto M, *et al*. The negative effect of preoperative transcatheter arterial chemoembolization on long-term outcomes for resectable hepatocellular carcinoma: a propensity score matching analysis. *Yonago Acta Med* 2016;59:270-278.
5 Choi SB, Kim KS, Park YN, *et al*. The efficacy of hepatic resection after neoadjuvant transarterial chemoembolization (TACE) and radiation therapy in hepatocellular carcinoma greater than 5 cm in size. *J Korean Med Sci* 2009;24:242–7.
6 Uchida M, Kohno H, Kubota H, *et al*. Role of preoperative transcatheter arterial oily chemoembolization for resectable hepatocellular carcinoma. *World J Surg* 1996;20:326–31.
7 Cheng A-L, Qin S, Ikeda M, *et al*. IMbrave150: efficacy and safety results from a pH III study evaluating atezolizumab (atezo) + bevacizumab (bev) vs sorafenib (SOR) as first treatment (tx) for patients (PTS) with unresectable hepatocellular carcinoma (HCC). *Annals of Oncology* 2019;30:ix186–7.
8 Llovet J, Shepard KV, Finn RS, *et al*. A phase Ib trial of lenvatinib (LEN) plus pembrolizumab (PEMBRO) in unresectable hepatocellular carcinoma (uHCC): updated results. *Annals of Oncology* 2019;30:v286–7.
9 Finn RS, Qin S, Ikeda M, *et al*. Atezolizumab plus bevacizumab in unresectable hepatocellular carcinoma. *N Engl J Med* 2020;382:1894–905.
10 Zhang J, Huang M, Cai Y, *et al*. Neoadjuvant chemotherapy with mFOLFOXIRI without routine use of radiotherapy for locally advanced rectal cancer. *Clin Colorectal Cancer* 2019;18:238–44.
11 Peyton CC, Tang D, Reich RR, *et al*. Downstaging and survival outcomes associated with neoadjuvant chemotherapy regimens among patients treated with cystectomy for muscle-invasive bladder cancer. *JAMA Oncology* 2018;4:1535–42.
12 Jackson HW, Fischer JR, Zanotelli VRT, *et al*. The single-cell pathology landscape of breast cancer. *Nature* 2020;578:615–20.
13 Stein-O'Brien GL, Clark BS, Sherman T, *et al*. Decomposing cell identity for transfer learning across cellular measurements, platforms, tissues, and species. *Cell Syst* 2019;8:395–411.
14 Van Gassen S, Callebaut B, Van Helden MJ, *et al*. FlowSOM: using self-organizing maps for visualization and interpretation of cytometry data. *Cytometry A* 2015;87:636–45.
15 Llovet JM, Fuster J, Bruix J, *et al*. The Barcelona approach: diagnosis, staging, and treatment of hepatocellular carcinoma. *Liver Transpl* 2004;10:S115–20.
16 Schapiro D, Jackson HW, Raghuraman S, *et al*. histoCAT: analysis of cell phenotypes and interactions in multiplex image cytometry data. *Nat Methods* 2017;14:873–6.
17 Kaseb AO, Carmagnani Pestana R, Vence LM, *et al*. Randomized, open-label, perioperative phase II study evaluating nivolumab alone versus nivolumab plus ipilimumab in patients with resectable HCC. *Journal of Clinical Oncology* 2019;37:185.
18 Irtan S, Chopin-Laly X, Ronot M, *et al*. Complete regression of locally advanced hepatocellular carcinoma induced by sorafenib allowing curative resection. *Liver Int* 2011;31:740–3.
19 Stein JE, Lipson EJ, Cottrell TR, *et al*. Pan-Tumor Pathologic Scoring of Response to PD-(L)1 Blockade 2019.
20 Helmink BA, Reddy SM, Gao J, *et al*. B cells and tertiary lymphoid structures promote immunotherapy response. *Nature* 2020;577:549–55.
21 Freeman GJ, Long AJ, Iwai Y, *et al*. Engagement of the PD-1 immunoinhibitory receptor by a novel B7 family member leads to negative regulation of lymphocyte activation. *J Exp Med* 2000;192:1027–34.
22 Blank C, Brown I, Peterson AC, *et al*. PD-L1/B7H-1 inhibits the effector phase of tumor rejection by T cell receptor (TCR) transgenic CD8+ T cells. *Cancer Res* 2004;64:1140–5.
23 Verzoni E, Ferro S, Procopio G, *et al*. Potent natural killer (NK) and myeloid blood cell remodeling by cabozantinib (Cabo) in pre-treated metastatic renal cell carcinoma (mRCC) patients (PTS). *Annals of Oncology*. ; 2018;29:viii312.

Integrated Immunological Analysis of a Successful Conversion of Locally Advanced Hepatocellular Carcinoma to Resectability with Neoadjuvant Therapy

SUPPLEMENTARY INFORMATION – METHODS

Trial design

This is an open-label single arm phase 1b study of neoadjuvant cabozantinib plus nivolumab in patients with borderline resectable or locally advanced HCC. Borderline resectable or locally advanced HCC was defined by, 1) Solitary tumor >5 cm, or 2) Unilobar multifocal disease either with >3 tumors or one tumor >3 cm, or 3) Bilobar disease with adequate future liver remnant, still technically resectable, or 4) High risk disease features (tumor >3 cm with macrovascular invasion or tumor >3 cm with AFP>400). Enrolled patients will receive a total of 8 weeks of cabozantinib therapy. After a two-week lead-in of cabozantinib monotherapy, patients receive concurrent nivolumab, one infusion every 2 weeks, for a total of 4 treatment doses. The primary endpoint is to characterize the safety and feasibility of preoperative cabozantinib plus nivolumab in locally advanced hepatocellular carcinoma (HCC).

Patient Samples

The evaluation of clinical samples was performed in accordance with the protocols approved by the Johns Hopkins Institutional Review Board (IRB). All specimens were obtained with written patient consent (IRB00149350). After receiving the surgical tumor tissue, mechanical mincing followed by enzymatic digestion in 0.1% collagenase in PBS at 37C for 30 minutes on an orbital shaker (60rpm) were performed. After centrifugation of the homogenate for 5 minutes at 1500rpm, the pellet was further processed using a Percoll gradient (GE Healthcare; 40% over 80% in PBS) centrifuged at 2000g for 25 minutes without break at room temperature (RT). The interface mononuclear layer was isolated into RPMI media. For peripheral blood samples, blood collection was done in two BD Vacutainer CPT – Cell Preparation Tube with Sodium Heparin and processed within two hours of collection. Tubes were centrifuged at RT for 30 minutes at 1800 rcf. Processed cells from tumor or blood were then counted and resuspended in AIM V (Gibco) and 10% DMSO. Cryovials were initially stored at -80C and transferred to liquid nitrogen for long term storage.

Antibodies

A list of Cytometry by Time-of-Flight (CyTOF) and Imaging Mass Cytometry (IMC) antibodies, isotopes, and concentrations used for immune cell subtyping is listed in Table S1 and S2, respectively. Conjugation of primary antibodies was performed using Maxpar Conjugation Kits according to the manufacturer's instructions. Briefly, purified antibodies were run through a buffer exchange protocol using 50kDa ultra filtration columns (Amicon) and then partially reduced with 4mM TCEP (Thermo Scientific). Polymers were loaded individually with isotopically enriched metals, 113In (Trace Sciences) and 115In (Sigma). Isotopically enriched Cisplatinum (194, 198) were directly conjugated onto the reduced antibodies (Mei, Leipold, & Maecker, 2016). Antibody concentrations in the wash buffer were quantified using Nanodrop. The final antibody concentrates were then diluted in a stabilization buffer (Candor) containing 0.3% sodium azide.

Cytometry by Time-of-Flight (CyTOF) Analysis

On the day of staining, peripheral blood samples were thawed rapidly in warm water bath and gently rinsed twice in RPMI media with 10% FBS and 1% penicillin-streptomycin according to standard protocols. Cells were rested at 37C in 5% CO2 for at least 30 minutes prior to further manipulation. To permit simultaneous analysis of cytokine production capacity, all samples were

stimulated in 1X PMA/ionomycin/brefeldin A cocktail (Biolegend) for 2.5 hours in complete media. Live/dead staining was performed with 5-minute incubation in 500nM palladium chloride (Sigma) dissolved in DMSO and diluted in PBS, subsequently quenched with complete media. For multiplexing samples, five different metals conjugated to CD45 antibodies were used for a "5-choose-3" scheme for a total of 10 possible unique barcodes (Hartmann, Simonds, & Bendall, 2018). Multiplexed samples were then incubated in Fc block (Invitrogen) for 10 minutes at RT. Surface marker staining was first done with chemokine receptor antibodies for 10 minutes at 37C, followed by the rest of surface markers for 30 minutes at RT. After two washes, intracellular staining was performed using Cytofix/Cytoperm kit (BD Biosciences) per manufacturer's protocol. Just before data collection, all cells were labeled with rhodium (Fluidigm) at 1:500 for 45 minutes at room temperature. All events were acquired on a Helios™ mass cytometer (Fluidigm). Randomization, bead normalization, and bead removal of data collected were performed on CyTOF software (Fluidigm) v6.7. Using FlowJo (BD) v10.5, single cell events were identified by gating based on cell length and rhodium signal. Dead cell filtering and debarcoding were performed by manually gating. For all CyTOF analyses, a computational pipeline based on diffcyt was employed using R v3.5 (Weber, Nowicka, Soneson, & Robinson, 2019). Briefly, for unsupervised clustering, FlowSOM algorithm was used to identify 30 meta-clusters that were then annotated into specific immune cell subtypes (Van Gassen et al., 2015). Clustering was visualized using a two-dimensional uniform manifold approximation and projection (UMAP) dimensionality reduction algorithm (Becht et al., 2019).

Imaging Mass Cytometry (IMC) Analysis

After constructing a tissue microarray (TMA) containing 1.5mm-diameter cores, including two from a deidentified normal liver and three from the patient described, it was dewaxed in xylene and rehydrated in alcohol gradient. The TMA slide was heated at 95C in Antigen Retrieval Agent pH 9 (Agilent) for 30 minutes. It was then blocked with 3% BSA in Maxpar PBS for 45 minutes at room temperature, followed by staining overnight at 4C with the antibody cocktail listed in Table S2. Ir-Intercalator in Maxpar PBS was used for DNA labeling. Images were acquired using a Hyperion Imaging System (Fluidigm) and data was preprocessed using a commercial software (Fluidigm). Image segmentation was performed using CellProfiler v.3.1.8. based on added image of Ir191 and Ir193 DNA staining, primary objects were identified using 5-15 pixel diameter (threshold strategy: global; method: minimum cross entropy; smoothing scale: 1.3488; correction factor 1.0) followed by secondary object identification with 3-pixel expansion. Resulting objects were converted to image in uint16 format. The single-cell segmentation mask was overlaid and the spatial information along with mean metal intensities of the markers were extracted into csv files. Individual files from each of the cores were converted into fcs files (https://github.com/sydneycytometry/CSV-to-FCS) to be input into the aforementioned computational pipeline. For neighborhood analysis, Single cell CoGAPS analysis (Stein-O'Brien et al., 2019) was performed on 26 mass intensities with the R/Bioconductor package version 3.5.8 to identify 13 patterns in these data. The PatternMarker statistic was applied to the inferred protein weights to define a set of unique protein markers associated with each pattern. The neighbors for each cell within surrounding 4 pixels were obtained using histoCAT (Schapiro et al., 2017). For each annotation in each core, the number of different cell-type and functional neighbors were calculated. The resulting numbers were combined for tumor and normal cores and the proportion of different neighbors were calculated. Moran's I autocorrelation coefficient was computed with R package ape version 5.3. To compute the autocorrelation coefficient, 10 nearest neighbors of each cell, computed based on the Euclidean distance of the geographic coordinates of each cell using FastKNN package version 0.0.1, were assigned a weight of 1 and the rest were assigned a zero weight.

SUPPLEMENTARY INFORMATION – RESULTS

Supplementary Figures 1-3
Supplementary Table 1

Supplementary Figure 1.

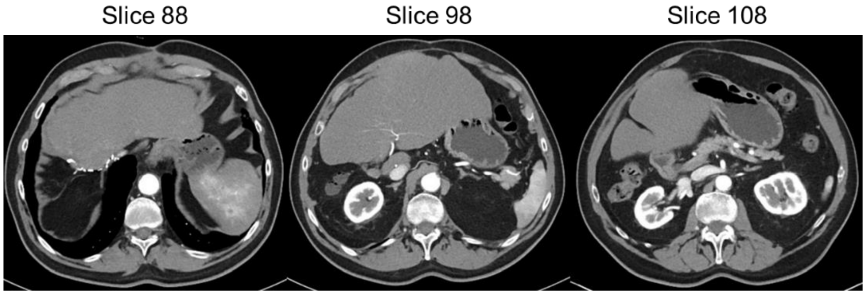

Three representative slices from the most recent CT scan (approximately 2 years from the date of the tumor resection) are shown.

Supplementary Table 1.

Timepoint	Total Prot g/dL	Alb g/dL	ALT U/L	AST U/L	Alk Phos U/L	Total Bili mg/dL	AFP ng/mL
At presentation	7.8	4.9	21	24	89	0.4	17,528.30
1 mo post-surgery	5	3.1	144	92	55	0.7	4.5
2 yr post-surgery	7.5	4.6	18	17	84	0.5	2.6

Liver function and AFP at presentation, 1 month post-surgery, and 2 years post-surgery

Supplementary Figure 2

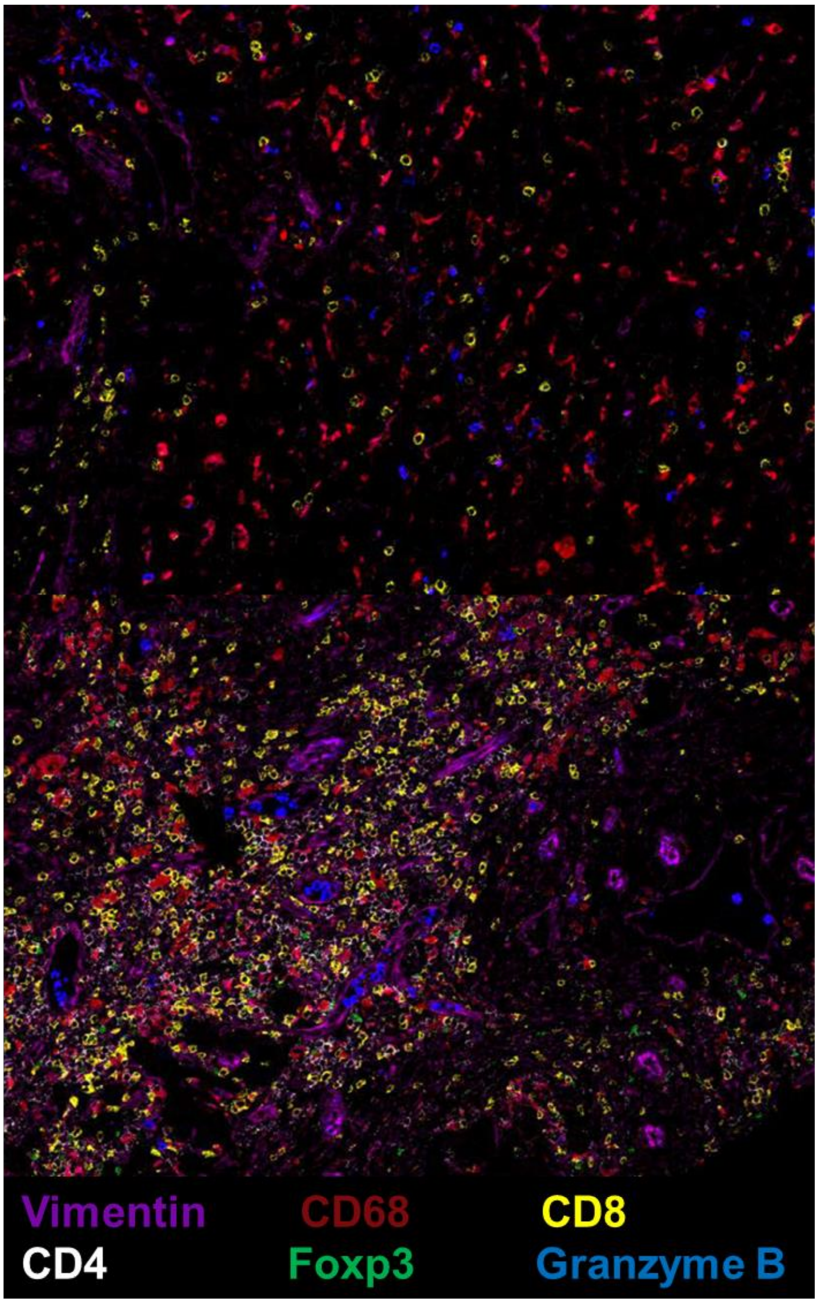

Higher resolution zoomed in images for IMC results for normal liver (Top) and surgically resected hepatocellular carcinoma (Bottom).

Supplementary Figure 3.

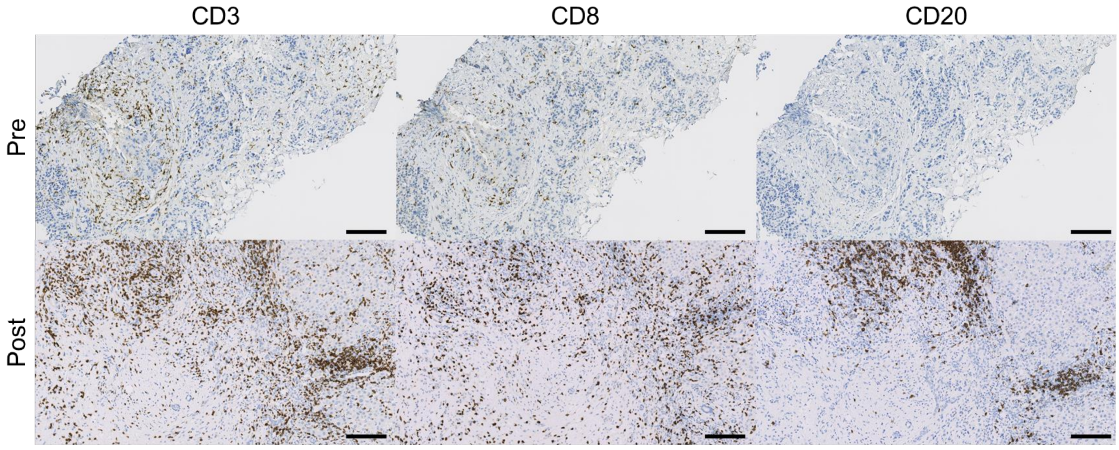

CD3 Density (cells/area mm^2)	CD8 Density (cells/area mm^2)	CD20 Density (cells/area mm^2)
Pre: 1175	Pre: 268	Pre: 32
Post: 1030	Post: 647	Post: 302

Representative single immunohistochemistry results against CD3, CD8, and CD20 in the tumor microenvironment between pre-treatment core biopsy and the post-treatment surgical resection samples. Quantified positive cell densities as determined by HALO are summarized in the table below. 10X magnification is shown (scale bar: 200μm).